DRAFT

Conceptual Design Report for Hall A Compton Polarimeter Upgrade

Sirish Nanda
Jefferson Laboratory
and
David Lhuillier
CEA-Saclay

February 12, 2004

Contents

1 Motivation **6**

2 Conceptual Design **8**
2.1 Photon Beam 8
2.1.1 Fabry-Perot Cavity 9
2.1.2 Laser 13
2.1.3 Transport Optics 19
2.1.4 Cavity Lock 19
2.2 Electron Detector 24
2.2.1 Present Setup 24
2.2.2 Microstrip Upgrade 24
2.3 Photon Calorimeter 25
2.3.1 Limitations of the present setup 25
2.3.2 Semi-integrated method 27
2.3.3 Integrated and energy weighted method 27
2.3.4 Calorimeter Upgrade 32
2.4 Data Acquisition 33

3 Expected Performances **33**
3.1 Coincidence Analysis 33
3.2 Integrated and energy weighted photon detection 38

4 Cost and Schedule **41**
4.0.1 Milestone Schedule 44

List of Figures

1 *Layout of the detection of the hall A Compton polarimeter.* 7
2 *Relative gain of the cavity as a function of the laser frequency in multiples of of the free spectral range ($\nu/\Delta\nu_{FSR}$ for different mirror finesse* 11
3 *The Gain, Reflectivity and Phase of the reflected light as a function of the deviation of frequency $\nu - \nu_0$ from the nearest resonance.* . . 12
4 *Heterodyne beat signal of two identical Prometheus lasers.* 15
5 *Frequency tuning behavior of the Prometheus laser with Nd:YAG crystal temperature.* 16
6 *Spectral distribution of the residual intensity noise for the Prometheus laser* 17
7 *Optics table of the green Compton polarimeter.* 20
8 *Schematic view of the PDH cavity locking* 21
9 *The reflected light intensity in the PDH cavity lock scheme with the incident laser beam modulated at 500 kHz* 22
10 *The PDH error signal near the resonance for small detune frequency* 23
11 *Fit of the experimental response to a photon flux of $125 \pm 7 MeV$, tagged by the 10th strip of the electron detector. The parametrization uses two Gaussian curves of different width on both sides of the maximum and a polynomial tail at low energy. Units on the horizontal axis are ADC channels.* 26
12 *Simulated response of a $6 \times 6 cm$ BaF2 crystal to 12.5 MeV photons. a):Spectrum of energy deposited as predicted by GEANT3.21. b): Same spectrum smeared by typical $PbWO_4$ resolution at that energy.* 28
13 *Mean analyzing power of the semi-integrated method ($\rho = 0.5$) versus statistical resolution of the photon calorimeter. The vertical axis is in % change relative to the "perfect" resolution case.* 29
14 *Top picture: Compton asymmetry (dotted curve) and energy weighted asymmetry (dash-dotted curve) versus photon energy for a green laser and $E_{beam} = 850$ MeV. On the same plot the mean (dashed curve) and mean energy weighted (solid curve) analyzing powers can be red with the horizontal axis standing for the detection threshold. Bottom picture: relative variation of the mean analyzing power in the low threshold region. The energy weighting reduces of lot the sensitivity to the position of the detection threshold.* 30
15 *Percentage of events depositing more than 250keV (circles), 500keV (squares) and 750keV (triangles) versus incident energy in a BaF2 crystal.* 31

16 $\delta A = (A_{Ei} - A_{Edet})/A_{Ei}$ *versus detection threshold for a 1.2 GeV beam and green laser (Compton edge at 49 MeV). A_{Ei} is the mean analyzing power weighted by the incident photon energy and A_{Edet} is weighted by the energy deposited in the detector. Left: $PbWO_4$ crystal of 1 R_M, Right: 2 R_M. The blue curves include the statistical smearing of the light yield of the detector.* 32

17 *Total relative error on the beam polarization for the semi-integrated method with the existing setup. The reference running conditions are taken from table 4 and evolution with beam energy follows the procedure described in the text. The monitoring error includes only the error not correlated from one run to another. The energy cut at 2.5 GeV is due to the limited operating range of the electron detector.* 35

18 *Expected performances of the semi-integrated method with the upgraded polarimeter. Solid curves are for a 40 minutes run, dashed curves are for 1 day. The envelope defined by two curves of the same type comes from the two different ways of evolving the response function error versus beam energy (see text for details).* 39

19 *Expected performances of the integrated and energy weighted method with the upgraded polarimeter. The beam energy is fixed at 850 MeV.* 42

List of Tables

1 *Relevant quantities of the Compton kinematics for the existing and proposed polarimeter setups. Y_{Det} is the vertical gap between the primary beam and Compton edge at the location of the electron detector. The following parameters are used: $I_{beam} = 50\mu A$, $P_e = 75\%$, $P_\gamma = 100\%$, $\sigma_e = 100\mu m$, $\sigma_\gamma = 100\mu m$ and $\alpha_{crossing} = 23.5\, mrad$. $< A >$ is the mean analyzing power with a detection threshold set to $\rho = k'/k_{max} = 0.5$. $< A_E >$ is the same quantity for the low threshold and energy weighted method.* 8

2 *Optical Cavity Specifications* 13

3 *Prometheus Laser Specifications* 18

4 Typical error budget of the "response function" analysis for a 40 minutes run with E=4.5 GeV, I=40 μA, $P_\gamma = 1500$ W and $\lambda = 1064$ nm. All errors are relative and $P_e \simeq 70\%$. The arrows indicate the expected error after the upgrade of the laser and the detectors with the same kinematics. 36

5 Typical error budget of a "integrated and energy weighed" measurement at 850 MeV with $P_\gamma = 3000$ W and $\lambda = 532$ nm. All other running conditions are identical to table 4. 41

6 *Cost Estimate* 43

Abstract

We propose a performance upgrade of the present Hall A Compton Polarimeter by doubling the laser frequency as well as the intra-cavity power with commercially available components. The existing Fabry-Perot cavity operating at 1064 nm (IR) with about 1.5 kW power will be replaced by a 532 nm (green) cavity with twice the power, resulting in a four-fold enhancement of the Figure of Merit ($\sigma < A >^2$) of the Compton polarimeter. Associated improvements to the electron detector, the photon calorimeter, and data acquisition method are likely to achieve 1% absolute accuracy of beam polarization measurement down to 0.85 GeV beam energy.

1 Motivation

The upgrade of the Compton polarimeter is motivated by upcoming high accuracy experiments with very demanding requirement on the beam polarization. Defining k the photon energy and E the electron beam energy, the Figure Of Merit (F.O.M.) of a Compton measurement scales with $k^2 \times E^2$, making high accuracy polarimetry a real challenge at low energy. The proposed upgrades are thus driven by the requirement of the Lead Parity experiment of 1% relative accuracy at 0.85 GeV. Sub-percent accuracy can be reached at higher beam energy although some limitations may show up from the operating energy range of the detectors. The best accuracy achieved so far is taken as a reference point to discuss the hardware upgrades and the expected error.

The present Compton setup allows the detection of both the scattered electrons and photons (Fig. 1). The most accurate analysis performed so far is reached in two steps. First we use coincidence data to determine the response function of the photon detector, the highly segmented electron detector being operated as an energy tagger. Then the polarimetry measurements rely on the photon detector only whose signal is integrated between a software threshold and the Compton edge. The experimental response function previously measured allows to compute the analyzing power with high precision.

A few mm safety gap must be kept between the electron detector and the primary beam (see section 2.2) leading to a low energy cut on the Compton spectrum. The experimental asymmetry and the analyzing power are thus extracted using a relatively high software threshold ($\rho = k'/k'_{max} \simeq 0.5$) above which all the systematics from detection are well under control. This method is called the "semi-integrated" or "response function" analysis. It has provided polarimetry measurements with 1.4% total error at 4.5 GeV and $40\mu A$ in a 40 minutes.[1]

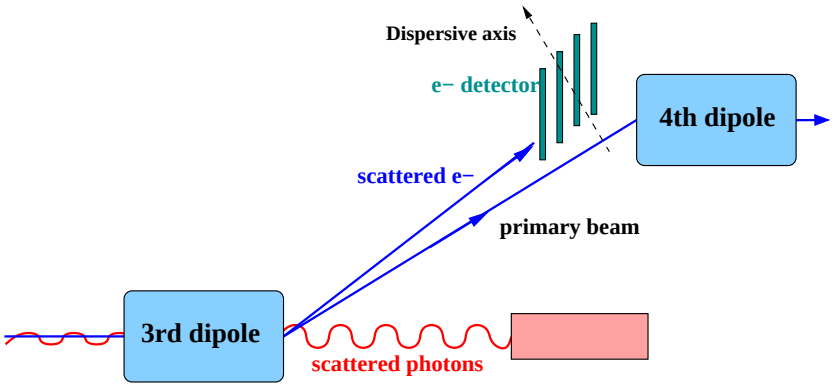

Figure 1: *Layout of the detection of the hall A Compton polarimeter.*

Table 1 shows the Compton scattering kinematics for a IR and a green laser and for 3 different beam energies. The figure of merit at $\lambda = 1064$nm is too low to meet the requirements of future high precision parity experiments in the 1 GeV range (PREX, Qweak). Therefore we present in the following section an upgrade of the laser setup to double the frequency and the power of the light accumulated in the optical cavity.

Two strategies are discussed for the detection of the Compton scattered particles:

- *Upgrade of the semi-integrated method*:
  Going to green doubles the separation between the scattered electrons and the primary beam (Table 1). Thus the electron detector can still be used to cover half of the Compton spectrum at 0.85 GeV and determine the response function of the photon detector.

- *Integrated and energy weighted photon signal*:
  A second method consists of weighing the photon signal by the energy deposited in the detector and integrate it over the whole Compton spectrum for each polarization state. Then the measured asymmetry can be written

$$A_E = \frac{E^+ - E^-}{E^+ + E^-} \tag{1}$$

  with

$$E^{\pm} = \mathcal{L}^{\pm} T^{\pm} \int_{\rho_{min}}^{1} E(\rho)\ \epsilon(\rho)\ \frac{d\sigma}{d\rho}(\rho)\ (1 \pm P_e P_\gamma A_l(\rho))$$

  E is the energy deposited in the calorimeter, ϵ the detection efficiency. Using a photon detector with a high light yield can bring the detection threshold ρ_{min} small enough with respect to the Compton edge so that it can be assumed to be negligible. Then the sensitivity to the detector response, main

Table 1: *Relevant quantities of the Compton kinematics for the existing and proposed polarimeter setups. Y_{Det} is the vertical gap between the primary beam and Compton edge at the location of the electron detector. The following parameters are used: $I_{beam} = 50\mu A$, $P_e = 75\%$, $P_\gamma = 100\%$, $\sigma_e = 100\mu m$, $\sigma_\gamma = 100\mu m$ and $\alpha_{crossing} = 23.5\, mrad$. $< A >$ is the mean analyzing power with a detection threshold set to $\rho = k^{'}/k_{max} = 0.5$. $< A_E >$ is the same quantity for the low threshold and energy weighted method.*

	$\lambda = 1064$ nm $P_L = 250$ mW, G=6000			$\lambda = 532$ nm $P_L = 100$ mW,30000		
E (GeV)	6.0	4.5	0.85	6.0	4.5	0.85
Y_{Det} (mm)	22.4	17.2	3.5	40.8	32.0	6.8
Lumi $(\mu barn.s)^{-1}$	0.206	0.206	0.206	0.206	0.206	0.206
$k'_{max}\,(MeV)$	582	335	12.7	1060	624	25.1
$\sigma\,(barn)$	0.592	0.609	0.654	0.538	0.563	0.642
Rate (kHz)	60.9	62.5	67.2	55.3	57.9	66.0
$< A >$ (%)	6.06	4.66	0.94	10.91	8.62	1.85
F.O.M. $(\sigma \times A^2)$	21.7	13.2	0.57	64.0	41.9	2.2
$< A_E >$ (%)	4.78	3.69	0.75	8.55	6.79	1.47
F.O.M. $(\sigma \times A_E^2)$	6.8	4.1	0.18	19.7	13.0	0.69

source of systematic errors, is highly reduced. This method could be implemented via a "HAPPEx like" acquisition system. In the case of a parity experiment, the polarimetry data would then be part of the same data flux. Very similar cuts could then be applied to the polarimetry and physics data, allowing an average over a long period of time with very small bias. The energy weighting is automatically implemented by the use of a thick calorimeter and keeps the analyzing power high, despite the low threshold. This method appears as a good compromise between a high analyzing power, comparable to the differential method, and a low sensitivity to the detection provided by the integration with low threshold.

2 Conceptual Design

2.1 Photon Beam

The relative merits of a single pass high power laser versus a high power Fabry-Perot cavity injected by a low power laser serving as the photon beam, has been extensively studied.[2] With commercially available solid state lasers, a cavity offers

superior luminosity and better control over systematic errors compared to single pass laser. Hence, our design choice for the photon beam is a high gain Fabry-Perot cavity. Our design goal is a green cavity with 3000 Watts of intra-cavity power. With 200 mW injection power, a cavity gain of 1.5×10^5 is required. Such a cavity represents the state of the art in cavity technology in the 532 nm region. Nonetheless, recent advances in the manufacturing of high reflectivity and low loss dielectric mirrors as well as availability of narrow line width green lasers facilitates the feasibility of our challenging design goal. High gain cavities at 532 nm have been successfully demonstrated by the KEK-ATF group [3] and very high gain super cavities are being planned[4]. Recently, the PVLAS[5] group have successfully constructed a 532 nm cavity with geometry and gain comparable to our proposed design here.

2.1.1 Fabry-Perot Cavity

We propose to trap the laser beam in a non-confocal Fabry-Perot resonator made of two highly reflective mirrors. The laser beam inside the cavity makes an infinite geometrical series of reflected and transmitted electromagnetic field. Assuming that the two mirrors are identical and are characterized by reflectivity r, transmissivity t, and absorption or other loss a and separated by a distance L, the cavity will resonate at the frequencies $\nu_m = mc/2nL$, where m is an integer, n is the refractive index of the medium, and c is the speed of light. The separation between two consecutive resonant frequencies called the "free spectral range" is then given by

$$\Delta\nu_{FSR} = \frac{c}{2L} \tag{2}$$

If the mirrors have high reflectivity, the resonance peaks are much narrower than $\Delta\nu_{FSR}$. The full-width at half-maximum of the resonance peak, referred to as the cavity-bandwidth, is given by

$$\delta\nu_{cav} = \frac{\Delta\nu_{FSR}}{F} \tag{3}$$

where $F = \pi\sqrt{r}/1-r$ is defined as the cavity "finesse."

Near resonance, the light power circulating in the cavity will be enhanced with respect to the incident Laser by a factor $G(\epsilon)$ which may be expressed as a function of the detuning parameter $\epsilon = (\nu - \nu_m)/\Delta\nu_{FSR}$ as

$$G(\epsilon) = G_0\frac{1}{1+(\frac{2F}{\pi})^2\sin^2(\pi\epsilon)} \tag{4}$$

where

$$G_0 = \frac{r}{(1-r)^2} \simeq \frac{F}{\pi} \tag{5}$$

is the maximum gain at $\epsilon = 0$. The cavity reflectivity is given by

$$R(\epsilon) \;=\; R\left[\frac{a^2 + 4(1-a)\sin^2\pi\epsilon}{(1-r)^2 + 4r\sin^2\pi\epsilon}\right] \tag{6}$$

and the phase Φ_R of the reflected field is given by

$$\tan\Phi_R(\epsilon) \;=\; \frac{t\sin 2\pi\epsilon}{1 - 2r\cos 2\pi\epsilon + r(r+t) - t\cos 2\pi\epsilon} \tag{7}$$

Shown in Fig. 2 is the cavity gain as a function of the laser frequency in multiples of of the free spectral range ($\nu/\Delta\nu_{FSR}$) for different values of finesse, with resonances occurring at integral values. Our design goal finesse of 49,000, requiring a mirror reflectivity of 99.9936%, is showin in solid line in the figure.

The cavity length will be 98 cm, so chosen as to be compatible with the existing Compton polarimeter setup in operation in Hall A. With this length, The free spectral range is a comfortable 153 MHz and the cavity bandwidth is 3.12 kHz.The main design parameters of the proposed cavity are given in Table 2. The variation of the gain, reflectivity and phase of the reflected light as a function of the deviation of frequency from the nearest resonance for the present design is shown in Fig. 3.

It is important to point out that several groups[5][6][7] have demonstrated cavity finesse from 45,000 to 220,000 in the 532 nm band. The matured ion beam sputtering technology has enabled the optics industry to produce ultra-high reflectivity mirrors. Research Electro Optics based in Colorado [9] has provided us with a quotation for supplying the mirrors meeting the high reflectivity and high damage-threshold (1 MW/cm^2) needed for our design. This firm has recently supplied high finesse mirrors to the PVLAS cavities and a number of other cavity projects. Measurements[5] indicate reflectivity exceeding 99.9997% and abosorption losses less than 2 parts per million in REO mirrors have been achieved.

The design goal of 3.12 kHz cavity bandwidth is narrower than the existing IR cavity which has a 4.9 kHz bandwidth. In order to maintain resonance in a consistent and reliable manner with such narrow bandwidths, a laser with narrow spectral line width and fast frequency tuning capability is necessary. In addition, a high bandwidth fast feedback servo system is required for frequency locking of the laser to the cavity. Both these aspects are discussed in the following sections.

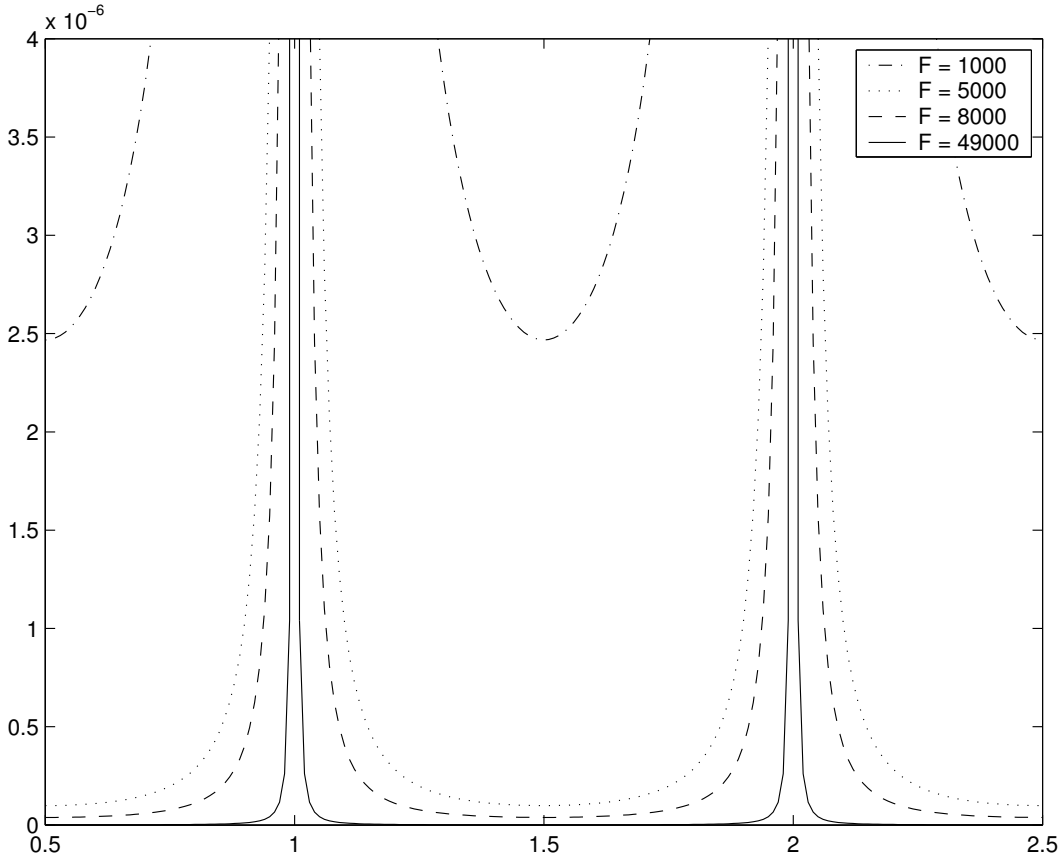

Figure 2: *Relative gain of the cavity as a function of the laser frequency in multiples of of the free spectral range ($\nu/\Delta\nu_{FSR}$ for different mirror finesse*

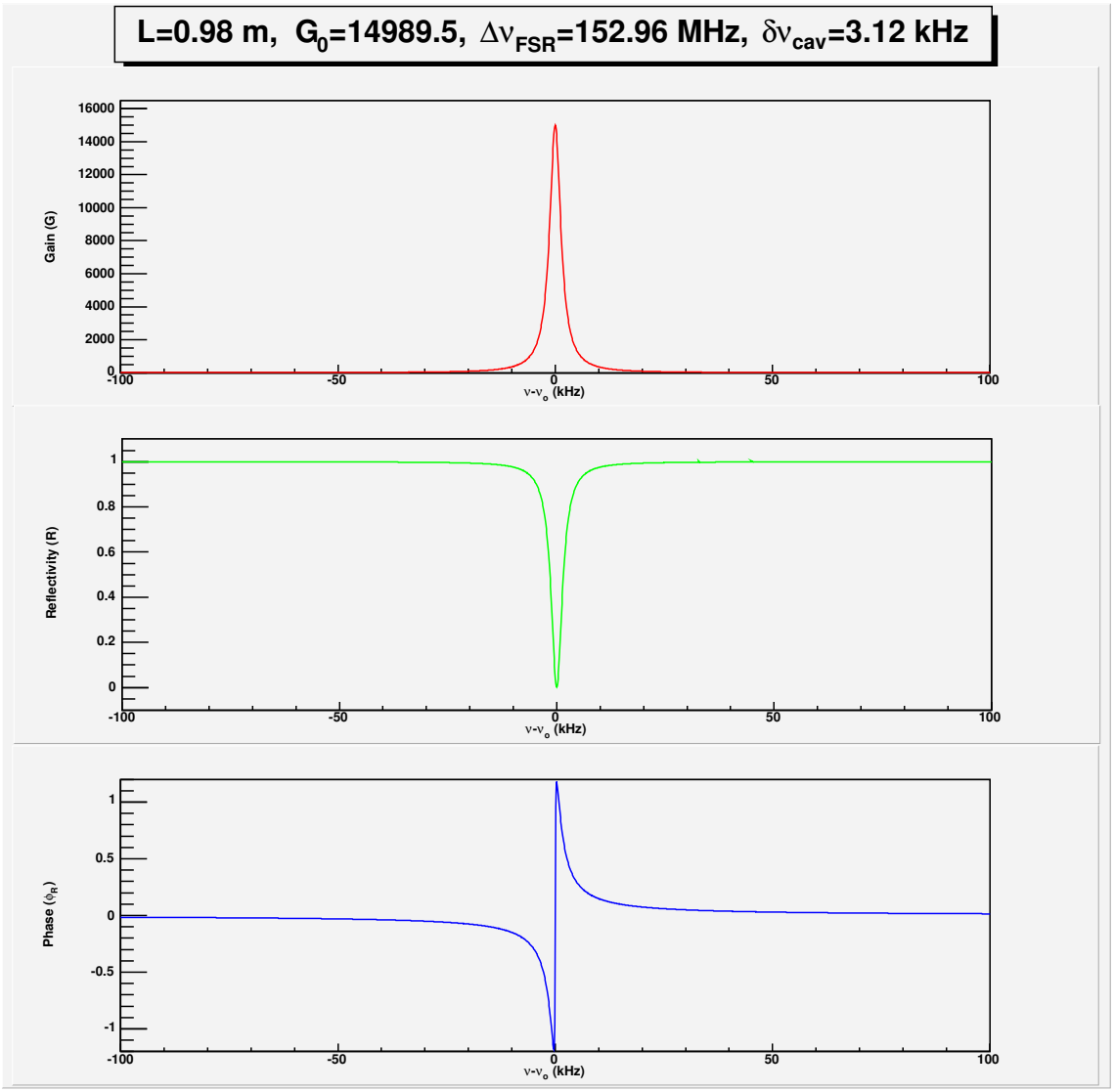

Figure 3: *The Gain, Reflectivity and Phase of the reflected light as a function of the deviation of frequency $\nu - \nu_0$ from the nearest resonance.*

Finally, the mechanical design of the cavity will be nearly identical to that of the existing infrared cavity. The cavity will be made from an Invar tube with static mirror mounts and ultra-high vacuum compatibility. Details of the mechanical design may be found in Ref.[2].

Table 2: *Optical Cavity Specifications*

Parameter	Symbol	Specification
Fabry-Perot Resonator		
Finesse	F	49,000
Power Gain	G	14,990
Q-factor	Q	1.8×10^{11}
Length	L	0.98 m
Free Spectral Range	$\Delta\nu_{FSR}$	153 MHz
Cavity Bandwidth	$\delta\nu_{cav}$	3.12 kHz
Beam Waist Size	σ	60 μm
Mirrors		
Type		Plano-Concave
Substrate		BK7
Radius of curvature	ρ	0.5 m
Diameter	d	7.75 mm
Thickness	t	4 mm
Coating		HR @532 nm 0^o concave face
		AR for planar face
Reflectivity	r	99.9936%
Loss	a	< 5 ppm
Damage Threshold		10 kW/mm^2, CW

2.1.2 Laser

We propose to use a Innolight Prometheus[10] laser which is a compact solid state diode-pumped, frequency-doubled Nd:YAG laser that provides single-frequency green (532 nm) continuous wave (CW) output of 100 mW. It offers superb spectral line with (1 kHz) of the green output and fast frequency tuning capability via a piezo-electric transducer (PZT). These features, essential for locking the laser beam to a high-finesse cavity, make the Prometheus an ideal choice for our design.

The Prometheus consists of a laser head and a power controller unit, connected by an umbilical cord. The laser head has three essential components: two

809 nm diode lasers providing the primary pump power, a Neodymium doped Yttrium Aluminum Garnet (Nd:YAG) crystal for 1064 nm infra-red generation, and a periodically-poled Potassium Titanium-oxide Phosphate (PPKTP) non-linear wave guide for second harmonic generation (SHG). The output of the pump diodes is coupled to the Nd:YAG crystal with focusing and mode-matching optics to excite the characteristic 1064 nm lasing wavelength of the Neodymium atoms. The Nd:YAG gain medium is a monolithic system forming a non-planar ring oscillator (NPRO). The high reflective mirrors of the resonator are directly coated to the polished faces of the NPRO crystal providing excellent stability of the infrared beam. A magnetic field is applied to the crystal to facilitate single unidirectional longitudinal mode (TEM_{00}) excitation. The pump diodes and the Nd:YAG crystal are temperature stabilized with thermoelectric coolers and precision temperature controllers in order to maximize the conversion efficiency to 1064 nm. Typically about 30% pump power is converted into infrared.

Since SHG coefficient in non-linear crystals tend be rather small, in order to have reasonable SHG output commercially available solid-state green lasers traditionally use a secondary resonating cavity with an intra-cavity frequency doubling crystal. The secondary cavity mirrors typically require internal feedback to maintain resonance, which tends to degrade the spectral line width and noise characteristics of the laser. In addition, such a scheme sacrifices the fast fast tuning capability of the laser frequency. In contrast, the Prometheus accomplishes SHG in a single pass through a quasi-phase matched PPKTP wave guide. Although conversion efficiencies are lower than a multi-pass doubling cavity, the spectral line width of the harmonic is virtually the same as the fundamental. Illustrated in Fig. 4 spectral line width of the Prometheus, measured by the heterodyning of two identical lasers. The non-linear PPKTP medium is also temperature stabilized to optimize SHG efficiency. The Prometheus can provide simultaneous dual frequency output, 1064 and 532 nm, phase-locked to each other.

The Prometheus offers two, slow and fast, modes of frequency tuning capabilities. Slow tuning is accomplished by changing the temperature of the Nd:YAG crystal. Shown in Fig. 5 is the thermal tuning behavior of the laser. The solid circles represent operation on a single frequency, while the open circles indicate mode-hops. The thermal tuning range at 532 nm is more than 60 GHz with a tuning coefficient of -6 GHz/C°. However, due the large time constant of a thermal process, the response bandwidth is less than a hertz.

Fast tuning of the Prometheus frequency is achieved by applying an external voltage to a PZT element attached to the Nd:YAG crystal. The PZT element can sustain response bandwidth more than 100 kHz while providing 20 MHz of tuning range. The PZT tuning input can, thus, be used in a fast feedback servo loop to lock the laser to an external high-finesse cavity. In addition, the same input can be utilized for modulating the frequency of the laser.

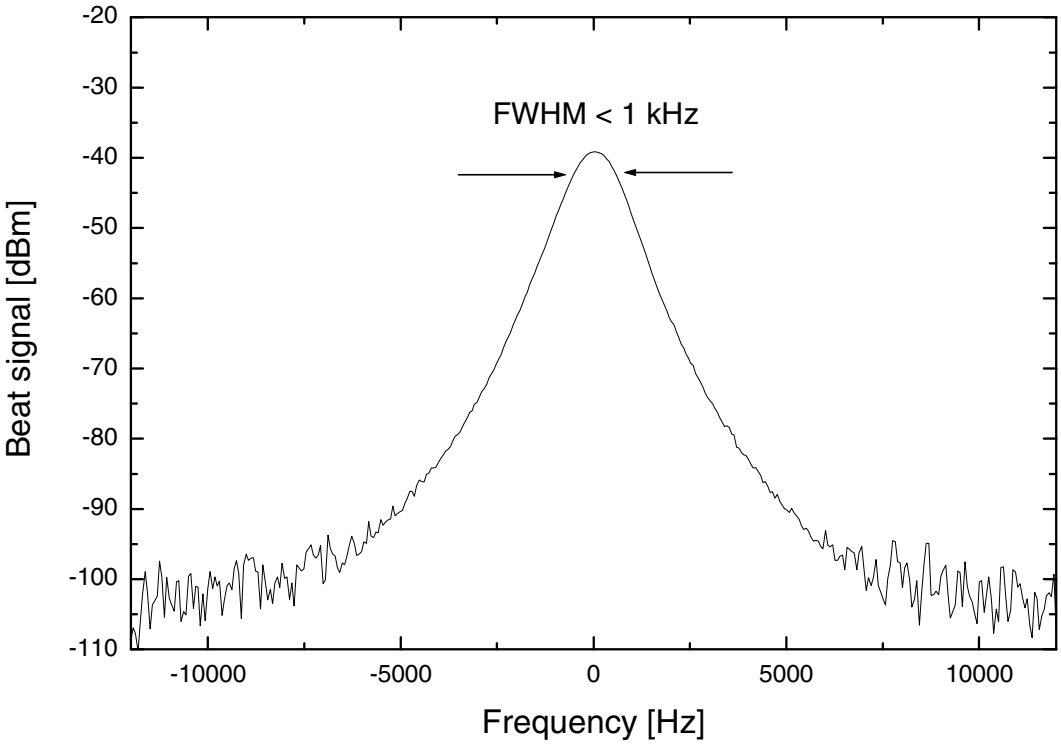

Figure 4: *Heterodyne beat signal of two identical Prometheus lasers.*

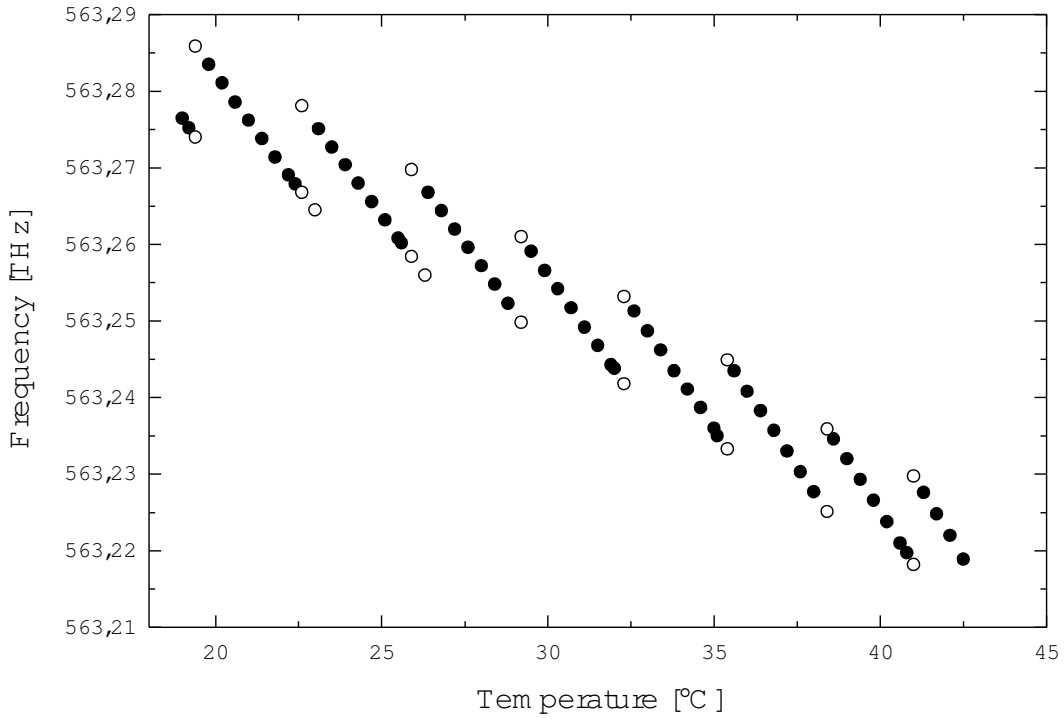

Figure 5: *Frequency tuning behavior of the Prometheus laser with Nd:YAG crystal temperature.*

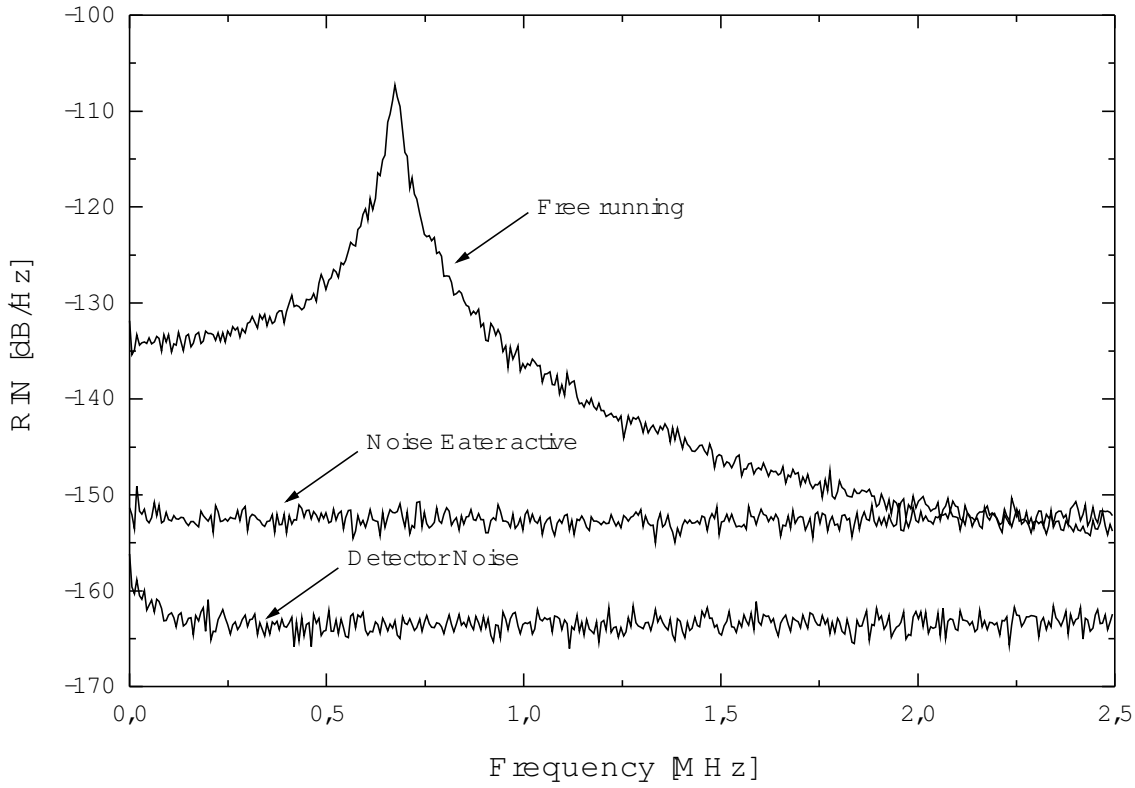

Figure 6: *Spectral distribution of the residual intensity noise for the Prometheus laser*

The Prometheus offers excellent noise characteristics. Illustrated in Fig. 6 is the spectral distribution of the residual intensity noise (RIN) of the laser. In free running mode the, the spike in the noise spectrum occurring at about 600 kHz is due to the relaxation oscillations of the NPRO crystal. This noise can be suppressed with a noise reduction mechanism that samples a fraction of the output beam and feeds an error signal back to the pump diode current. With this "noise eater" option the RIN of the Prometheus is close to the shot noise limit of most photo diode detectors.

Table 3: *Prometheus Laser Specifications*

Wavelength	532	nm
Output Power	100*	mW
Mode	TEM_{00}	
Beam roundness (M^2)	< 1.1	
Beam diameter	0.38	mm
Beam divergence	2.8	mrad
Polarization	$>$ 100:1	
Thermal tuning coefficient	-6	GHz/K
Thermal tuning range	60	GHz
Thermal response bandwidth	1	Hz
PZT tuning coefficient	2	MHz/V
PZT tuning range	$\pm$200	MHz
PZT response bandwidth	100	kHz
Spectral line width	1	kHz/100 ms
Coherence length	$>$1	km
Frequency drift	2	MHz/min
Relative Intensity Noise (RIN)	$>$ -90	dB/Hz
Noise eater option RIN	$>$ -140	dB/Hz

*Initial power. Power will be upgraded to 200 mW

The specifications of the Prometheus laser are shown in Table.3. The Prometheus is presently offered at 100 mW power in the green. However, although not commercially offered yet, it can be upgraded in the near future to 200 mW. We plan to start with the 100 mW version for bench tests and prototype development of the cavity system. The injection power requrement for the final design will be decided based on the actual gain achieved in the prototype cavity.

2.1.3 Transport Optics

Details of the transport optics will be fixed by the study of the cavity in test setup. In this section we give a tentative list of the optical elements based on the existing setup. Figure 7 illustrates the main blocks required along the laser line:

- Linear polarization: A set of polarizers purifies the linear polarization of the laser.

- Remote laser intensity control: A half wave plate and an extra polarizer can provide a remote intensity control, useful for the study of the systematics associated with dead time and pile up.

- Remote polarization reversal: The reversal of the photon polarization is driven by a rotatable quarter-wave plate. A Pockels cell could be used for a higher reversal frequency depending on the feedback stability and locking time.

- Focusing and steering control: The laser beam waist at the C.I.P. is fixed by a set of lenses. The coupling of the laser beam to the cavity optical axis is optimized by remote controlled mirrors. Effect of birefringence is reduce by the couples of mirrors rotating around perpendicular axis.

- Remote polarization monitoring: A polarization analyzing line similar to the existing one is proposed to monitor the polarization of the laser.

2.1.4 Cavity Lock

The cavity in our design has fixed mirrors in a stable enclosure. Nonetheless, thermal and acoustic noise will introduce fluctuations in the cavity length far in excess of the cavity bandwidth. Hence, a dynamic feedback loop is necessary to constantly adjust the laser frequency to follow changes in cavity length. We plan to implement the well proven Pound-Drever-Hall[11] (PDH) method to lock the laser to the cavity. As shown in Fig. 3 the phase of the reflected light Φ_R, near resonance, is proportional to the detune frequency and goes through a zero crossing on resonance. Hence, Φ_R can be used as an error signal in a feedback loop. The PDH scheme provides a method of determining Φ_R by measuring the phase difference between frequency modulated sidebands and the main carrier in the power reflected by the cavity. A schematic view of the proposed PDH lock set up is shown in Figure 8. The formalism of reflection of phase modulated light from a cavity have been discussed extensively elsewhere.[11][8][2] Here we cover the essential features. Before injection to the cavity the laser light is phase

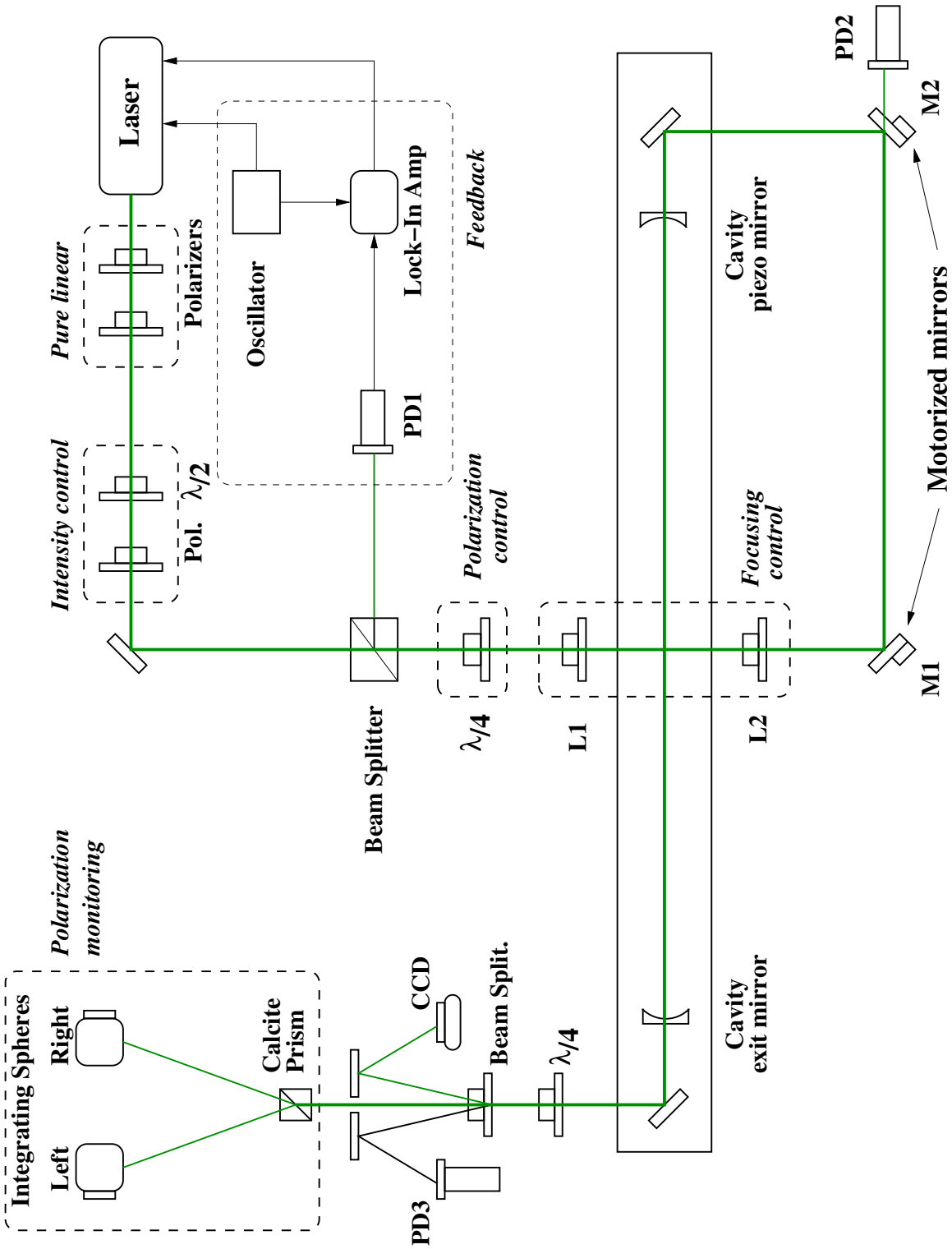

Figure 7: *Optics table of the green Compton polarimeter.*

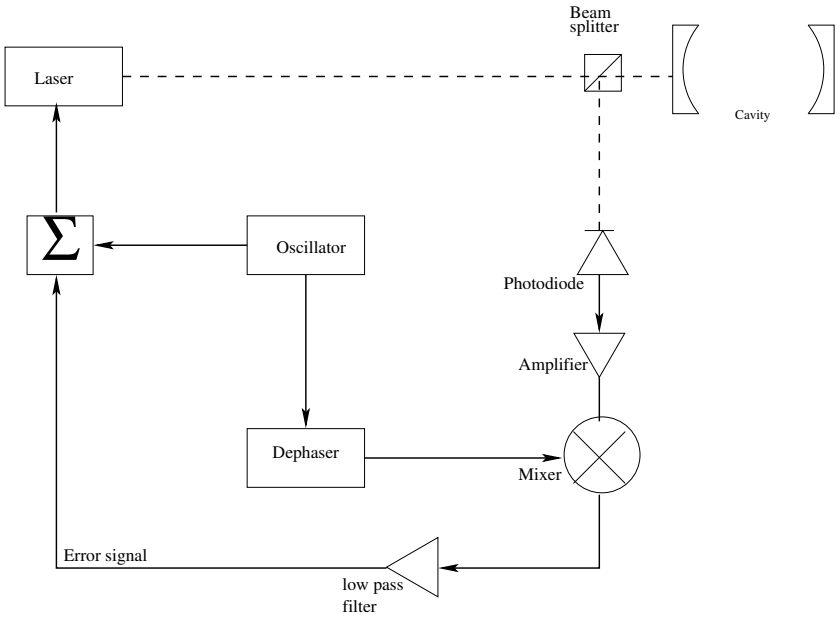

Figure 8: *Schematic view of the PDH cavity locking*

modulated by a local oscillator at a frequency Ω with a modulation amplitude m. The modulated light field is then given by

$$E_I = E_o e^{i\omega t} e^{im\cos(\Omega t+\Phi_\Omega)} \tag{8}$$

where $\omega = 2\pi\nu$. Alternatively, the incident field can be expanded as a series of Bessel functions:

$$E_I = E_o \left[J_o(m) e^{i\omega t} + [\sum_{k=1}^{\infty} J_k(m)(e^{ik(\frac{\pi}{2}+\Phi_\Omega)} e^{i\omega_k^{+t}} + e^{ik(\frac{\pi}{2}-\Phi_\Omega)} e^{i\omega_k^{-t}})] \right] \tag{9}$$

which gives the reflective field as

$$\begin{aligned} E_r = {} & E_o e^{i\omega t}[J_0(m)\sqrt{R(\omega)} e^{i\Phi_R(\omega)} \\ & +(i)J_1(m)\sqrt{R(\omega+\Omega)} e^{i\Phi_R(\omega+\Omega)} e^{+i(\Omega t+\Phi_\Omega)} \\ & +(i)J_1(m)\sqrt{R(\omega-\Omega)} e^{i\Phi_R(\omega-\Omega)} e^{-i(\Omega t+\Phi_\Omega)}] \end{aligned} \tag{10}$$

A fraction of the intensity of the reflected field is sent to a photo-diode via a beam splitter as shown in Fig. 8. After amplification the photo-diode voltage is mixed

with the local oscillator frequency. The voltage output from the mixer is then sent to a low pass filter. This cuts all frequencies above Ω and results in DC voltage output as follows:

$$\begin{aligned} V_{err} \quad \propto \quad & E_o J_o(m) J_1(m) \sqrt{R(\omega)} \\ & [\sqrt{R(\omega+\Omega)} \sin(\Phi_R(\omega+\Omega) - \Phi_R(\omega) + (\Phi_\Omega - \Phi_{\Omega_M})) \\ & + \sqrt{R(\omega-\Omega)} \sin(\Phi_R(\omega-\Omega) - \Phi_R(\omega) - (\Phi_\Omega - \Phi_{\Omega_M}))] \end{aligned} \tag{11}$$

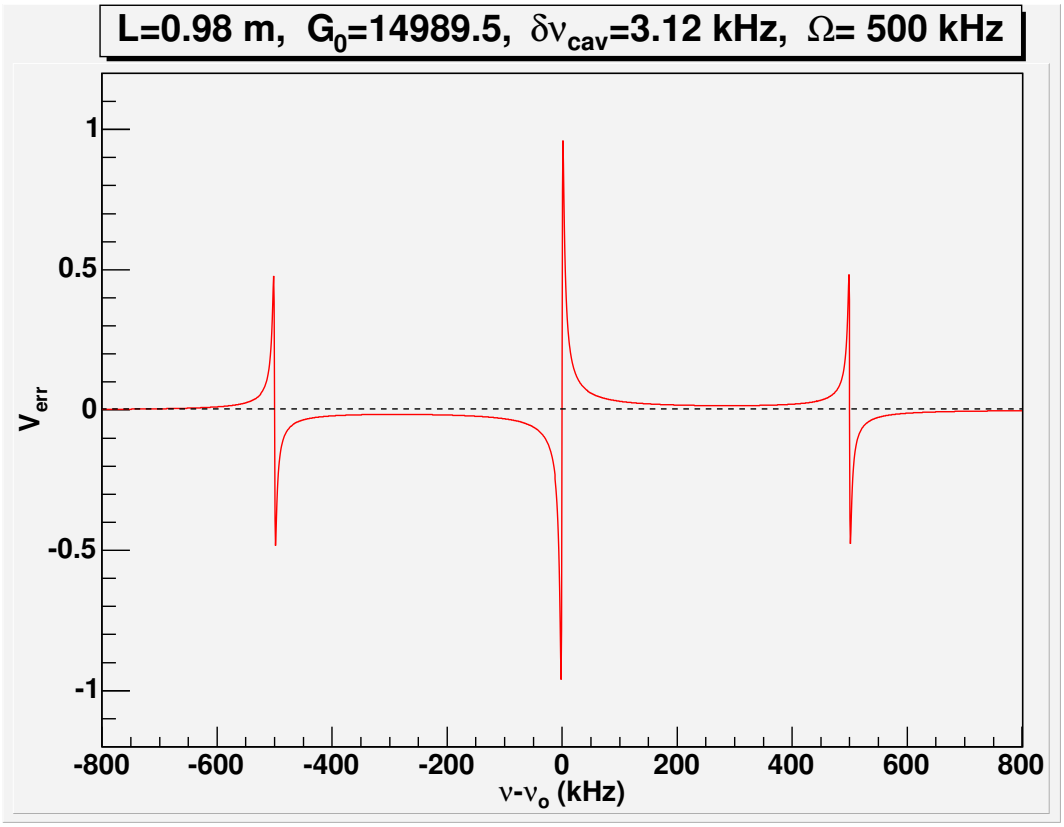

Figure 9: *The reflected light intensity in the PDH cavity lock scheme with the incident laser beam modulated at 500 kHz*

If Ω is chosen so that

$$\Delta\nu_{FSR} \ll \Omega/2\pi \ll \delta\nu_{cav}$$

V_{err} as shown in Fig. 9 as a function of detune frequency from the nearest resonance, shows two clear side bands with opposite phase compared to the main carrier. Very near the resonance, $R(\omega \pm \Omega)$=1 and $\Phi_R(\omega - \Omega)$=0, Eq.11 simplifies to

$$V_{err} \quad \propto \quad E_o J_o(m) J_1(m) \sqrt{R(\omega)} \sin(\Phi_R(\omega)) \tag{12}$$

The near resonance behavior of V_{err} as a function of detune frequency is shown in Fig. 10. Clearly, this signal forms an ideal candidate for an error signal for the feedback loop servo system. The heart of the servo system is a Signal Recovery

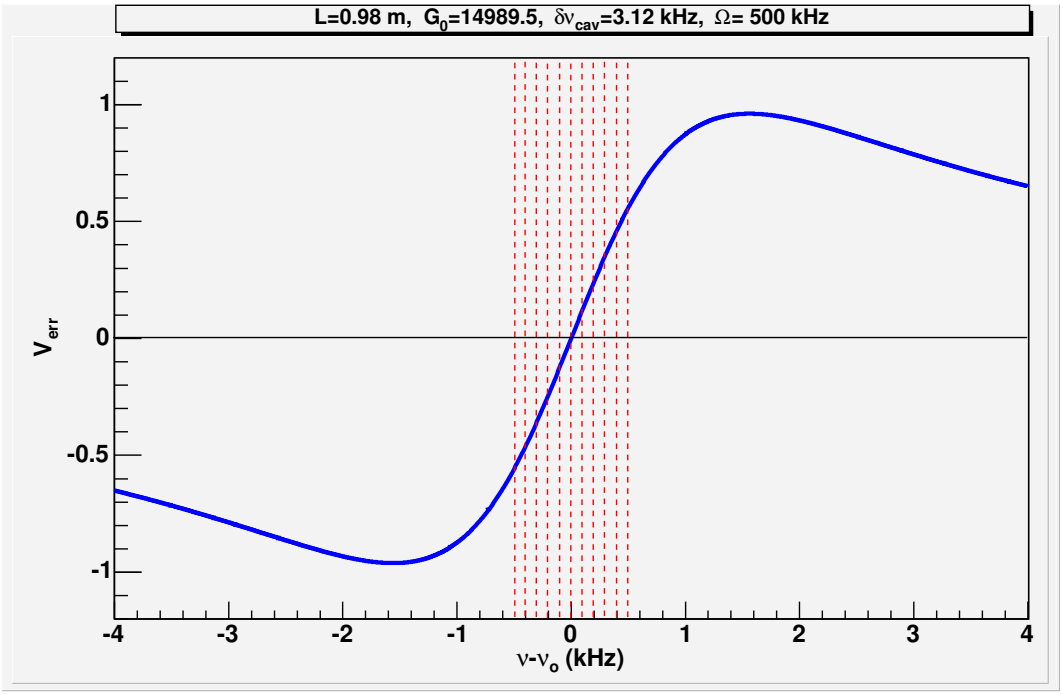

Figure 10: *The PDH error signal near the resonance for small detune frequency*

7280 lock-in amplifier. The PZT "fast" frequency tuning input of the Prometheus will be used for both frequency modulation and error signal from the servo system. Frequency modulation of the laser and reference signal for the lock-in amplifier is provided by a Yokogawa FG200 oscillator. Our choice of $\Omega = 500$ kHz is based on the experience of the PVLAS group[**?**, bregant] However, the final value will be decided after a careful study of the spectral distribution of the intensity noise and residual amplitude modulation with the actual laser delivered to us. In addition, an HP 33120A slow ramp generator will be used to scan the "slow" thermal tuning range of the Prometheus in order to get close to a resonance where the servo system can operate.

2.2 Electron Detector

2.2.1 Present Setup

The electron detector is located a few mm above the primary beam between the 3^{rd} and the 4^{th} dipoles of the magnetic chicane (Fig. 1). The active part consists of 4 planes of 48 silicon micro-strips, segmented along the dipole dispersive axis in bins of $650\mu m$. The energy of the Compton scattered electron is directly related to its measured position in the detector. Thus the high segmentation gives a very good energy resolution of the order of 0.2% of the beam energy. The absence of dead zone and the redundancy of the 4 planes make the detection efficiency close to 100%.
The main systematic error comes from the energy calibration which is directly connected to the error on the position along the dispersive axis. When using the electron data only, the effect on the polarization measurement is enhanced by a factor 2 due to the quadratic dependence of the Compton edge on the beam energy

$$\Delta P_e/P_e = 2 \times \Delta Y/Y \tag{13}$$

where Y is the distance between the Compton edge and the primary beam.
From data taken with 3 active planes the uncertainty on the vertical position is 200 microns.

2.2.2 Microstrip Upgrade

To first order, reducing the strip size, $\Delta P_e/P_e$ can be reduced in proportion to the strip size and micro-strips as narrow as $20\mu m$ are available on the market. However, experimental constraints prevent the error on the position to simply scale with the strip size. The main limitation comes from the fact that the laser and electron beam spot sizes can't be made arbitrarily small at the Compton Interaction Point ($\geq 100\mu m$). In addition we want to keep 48 channels per plane with the same front end electronics in order to reduce the cost of the upgrade. Going to very small strip size would then shrink the active area of the detector and define a too narrow operating range in beam energy. Therefore our goal is to achieve a 150 μm resolution on the vertical position of the scattered electrons using 300 μm wide micro-strips.
At 850 MeV, the edge of the Compton spectrum is expected to stand at 6.8 mm above the primary beam (see table 1). From Eq.13 the calibration induces a 4.5% relative error on the beam polarization which is way above the required accuracy for the lead parity experiment. As already mentioned the way to reduce our sensitivity to energy calibration is to use the so-called "response function" analysis which has provided the best accuracy so far. This method consists of measuring the response function of the calorimeter using the electron detector as a photon energy tagger.

Since the parameters of this response function vary slowly with the incident photon energy the calibration error from the electron detector has a much smaller effect on the mean analyzing power.
In order to optimize the statistical and systematic errors, a software threshold close to $\rho = k'/k_m ax \simeq 0.5$ is applied on the data. Measuring the response function with such a threshold at 850 MeV requires detection of Compton scattered electrons between 6.8 and 3.4 mm away from the primary beam (Table 1). This is equivalent to a Compton photon energy range of 12 to 25 MeV. The issue of the parametrization of the response function in this energy range is discussed in the next section.
Another issue is the sensitivity to the beam halo which has to be below 10^{-10} of the beam intensity to be smaller than the Compton rate. Data taken in May 2003 with the electron detector at 3mm only above the primary beam showed a beam-halo at the 10^{-9} level at 3mm and 10^{-10} at 6mm. We believe the major part of this halo comes from the fact that the diode laser at the source doesn't turn off completely between two beam pulses, leading to leakage from one hall to another. From extrapolation of data taken in 2001 with a Ti-Saphire laser we believe this background can be reduced by an order of magnitude thus meeting our requirements.
A remote control of the vertical position of the electron detector would be of great help for the measurements at low beam energy. It could be implemented by rotating the electron detector setup by 90 degrees around the beam axis. This way the step motor could be used to move the strip vertically instead of horizontally in the present setup. Aside the optimization of the safety gap the vertical motion would also expand the maximum operating beam energy (Compton edge in the last strip) from 2.5 to around 5 GeV.

2.3 Photon Calorimeter

2.3.1 Limitations of the present setup

The present photon calorimeter has shown good performances at photon energies of 50 MeV or higher. With a green laser this correspond to beam energies $\geq$2GeV. In that range, the interactions of the photons with a dense detector are dominated by the e^+e^- pair creation process. The high multiplicity of the secondary particles leads to a Gaussian distribution of the deposited energy with a tail at lower energy due to leakage of the electromagnetic showers in the back and on the side of the calorimeter (Fig. 11).

The main systematic errors of the semi-integrated method are from the calibration of the electron detector, the parametrization of the response function and

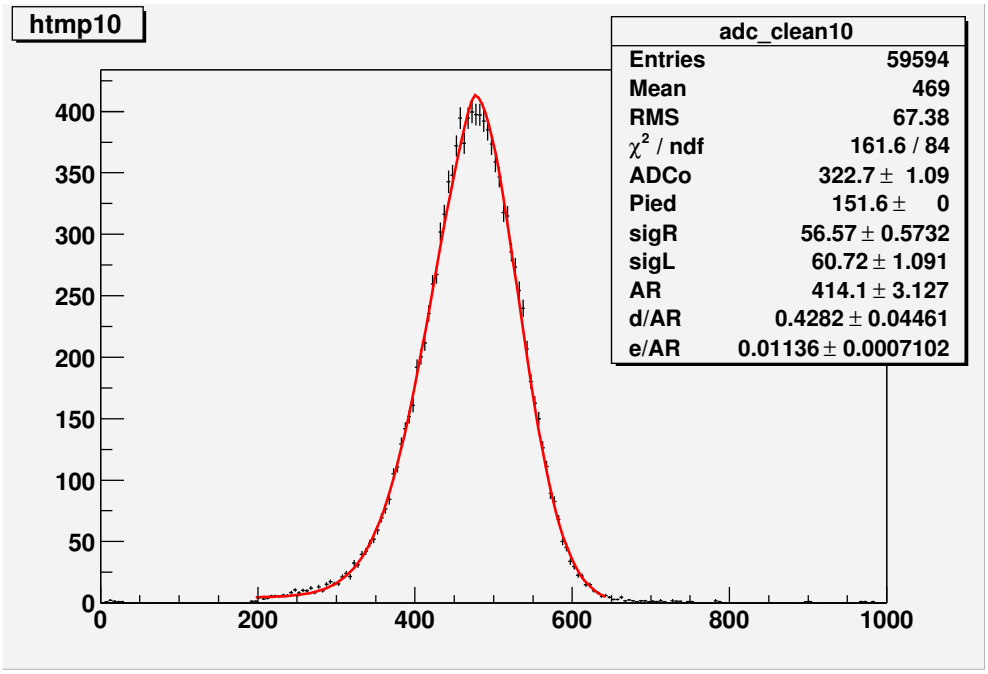

Figure 11: *Fit of the experimental response to a photon flux of* $125 \pm 7 MeV$*, tagged by the 10th strip of the electron detector. The parametrization uses two Gaussian curves of different width on both sides of the maximum and a polynomial tail at low energy. Units on the horizontal axis are ADC channels.*

the pile up (table 4). The calibration is improved by the upgrade proposed in the previous section. A better control of the parametrization of the response function can be achieved by using a calorimeter of larger transverse dimensions as compared to the existing $2 \times 2 \times 23\,cm^3$ $PbWO_4$ crystal. The scale is given by the Molière radius ($R_M = 2.2\,cm$ for $PbWO_4$) and large means $\geq 2R_M$. This would significantly reduce the low energy tail which at present is parametrized by an *ad hoc* polynomial. This way the response function would be closer to a Gaussian providing physical constraints on the kind of parametrization to be used. Finally the effect of pile up is directly proportional to the laser power and beam current. The F.O.M. of Compton polarimetry with a green laser and $E_{beam} \geq 2$GeV is good enough so that studies or measurements can be performed at reduced luminosity.

2.3.2 Semi-integrated method

At beam energy as low as 850 MeV and with a green laser, the Compton edge of the photon spectrum is at 25MeV only. In this energy range the response function of the calorimeter is expected to be much more complex because Compton scattering inside the detector starts to play an important role. This is illustrated in figure 12-a. In the limit of perfect resolution several peaks spaced out by $E = m_e c^2 = 0.511 MeV$ appear in the spectrum of deposited energy. They correspond to the full-energy peak, single escape peak, double escape peak,... The rest of the spectrum is populated by multiple Compton scattering. Taking into account the observed $PbWO_4$ resolution smears out this peak structure (Fig. 12-b) but then the mean analyzing power above $\rho \simeq 0.5$ decreases and is much more sensitive to the accuracy with which the resolution is known (Fig. 13).

Thus the semi-integrated method is still possible at low energy with the upgrades of the laser and the electron detector but the systematic errors are potentially high, depending on the compromise between the resolution of the calorimeter and the parametrization of the response function. The pile up may also become an issue since the very slow statistical convergence at low energy will require the maximum luminosity.

2.3.3 Integrated and energy weighted method

Another option is the integrated and energy weighted method (Eq.1). In that case the main requirements for the photon detector are:

- *A large light yield to allow small detection threshold*: Figure 14 shows that for the integrated and energy weighted method the slope at the origin of the

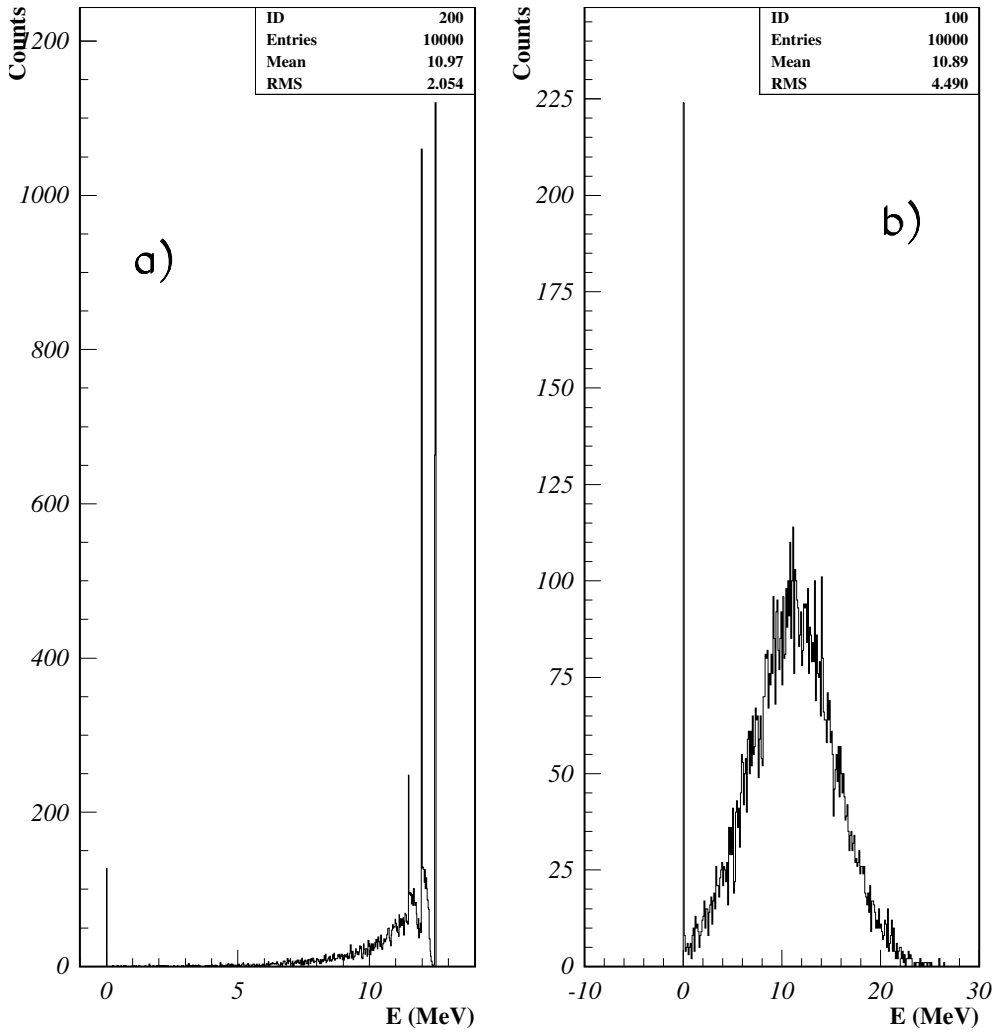

Figure 12: *Simulated response of a* $6 \times 6cm$ *BaF2 crystal to 12.5 MeV photons. a):Spectrum of energy deposited as predicted by GEANT3.21. b): Same spectrum smeared by typical* $PbWO_4$ *resolution at that energy.*

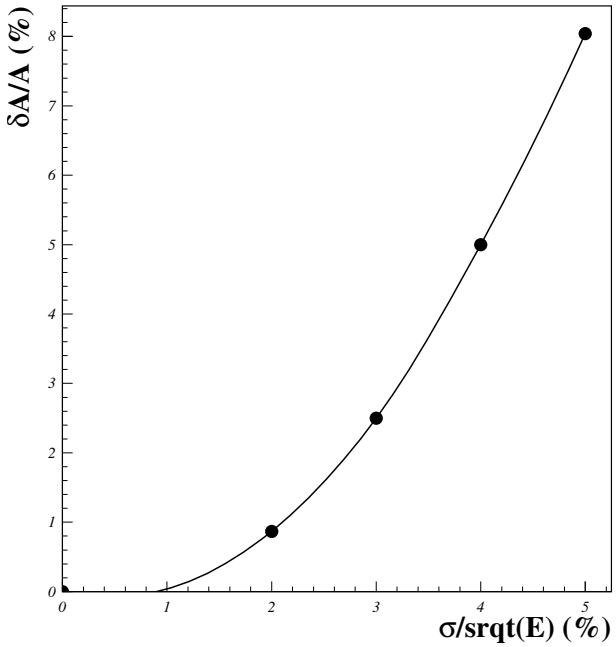

Figure 13: *Mean analyzing power of the semi-integrated method ($\rho = 0.5$) versus statistical resolution of the photon calorimeter. The vertical axis is in % change relative to the "perfect" resolution case.*

mean analyzing power versus threshold is very flat. At $E_{beam} = 850$MeV the detection threshold can be anywhere between 0 and 1MeV and still have a negligible effect on the analyzing power ($\delta A/A = 0.25\%$ for 1MeV whereas it corresponds to 4% of the compton edge). Such a detection threshold is too low for the $PbWO_4$ but is definitely in the range of numerous inorganic scintillators (BGO, NaI, CsI, BaF2,...).

- *A good detection efficiency.* Figure 15 shows that with a dynamic range of 100 (0.25 to 25 MeV), the detection efficiency can be kept high and flat from 1 MeV until the Compton edge thus reducing the associated systematic errors. Measurements with radioactive sources can be performed in the low energy region, where the efficiency starts decreasing.

- *A large fiducial volume.* The detector should have many radiation lengths in depth and 2 R_M in the transverse dimension to contain the maximum of the shower.

Because of the typical integration gate of 33ms, no stringent constraint on the time response is required. From preliminary simulations it also turns out that the integrated method is little sensitive to the response function of the photon detector

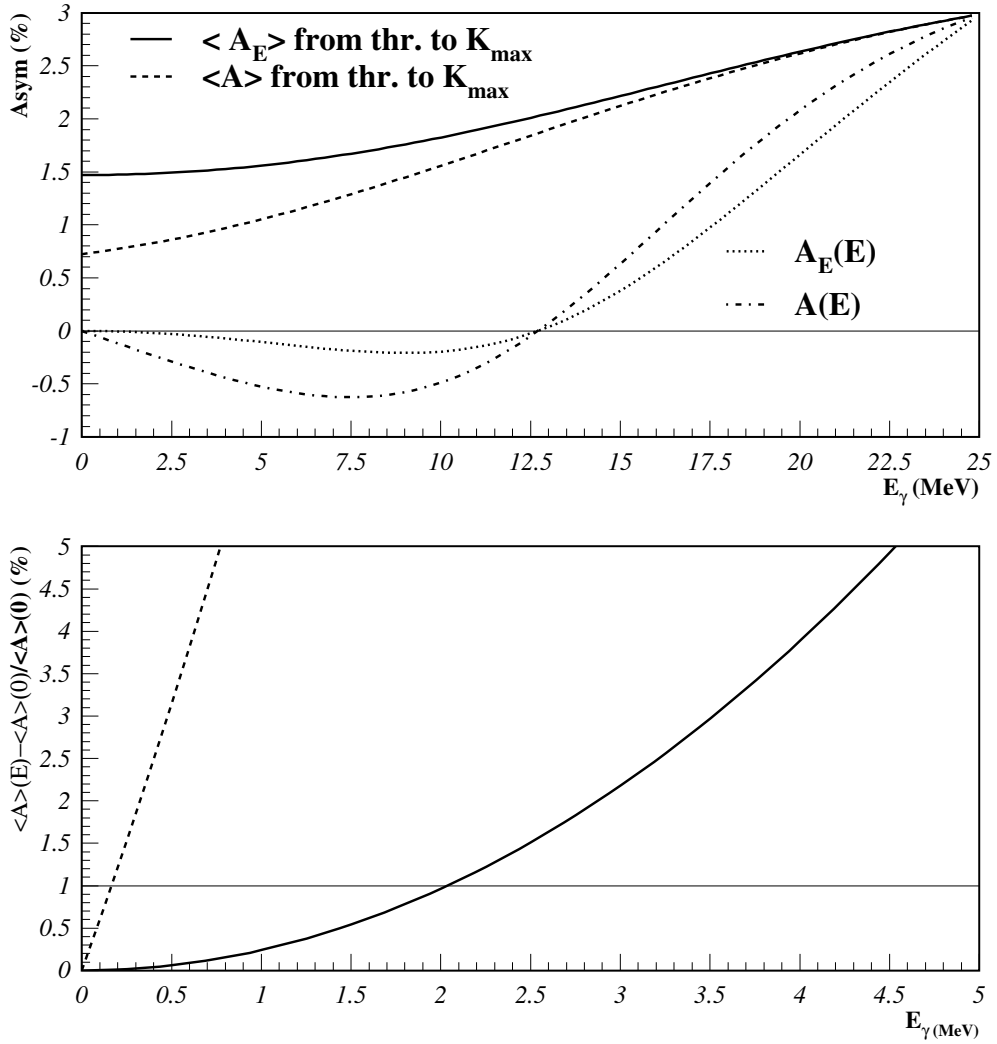

Figure 14: *Top picture: Compton asymmetry (dotted curve) and energy weighted asymmetry (dash-dotted curve) versus photon energy for a green laser and* $E_{beam} =$ 850 *MeV. On the same plot the mean (dashed curve) and mean energy weighted (solid curve) analyzing powers can be red with the horizontal axis standing for the detection threshold. Bottom picture: relative variation of the mean analyzing power in the low threshold region. The energy weighting reduces of lot the sensitivity to the position of the detection threshold.*

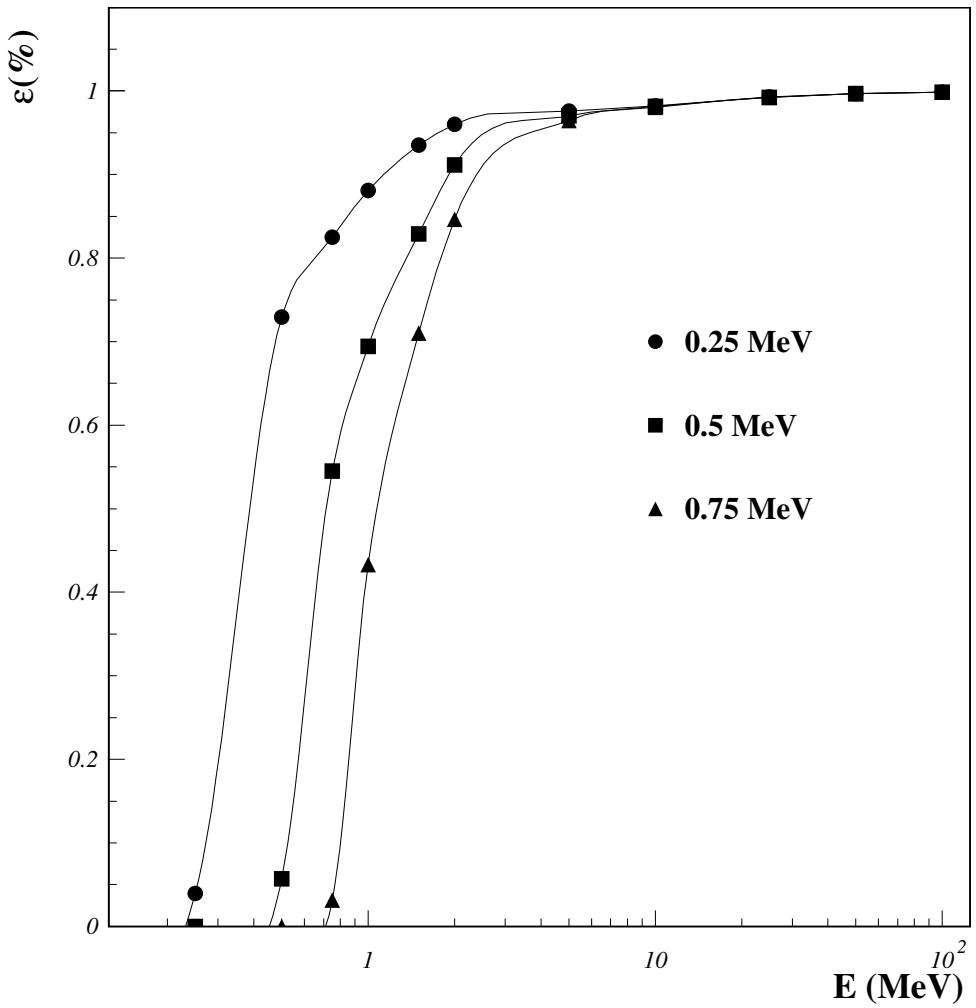

Figure 15: *Percentage of events depositing more than 250keV (circles), 500keV (squares) and 750keV (triangles) versus incident energy in a BaF2 crystal.*

(Fig. 16). Even a rough parametrization of the response function should be able to keep the systematic error well below the percent level. The same requirement for the non-linearity of the detection chain over the whole dynamic range gives a limit of 3%.

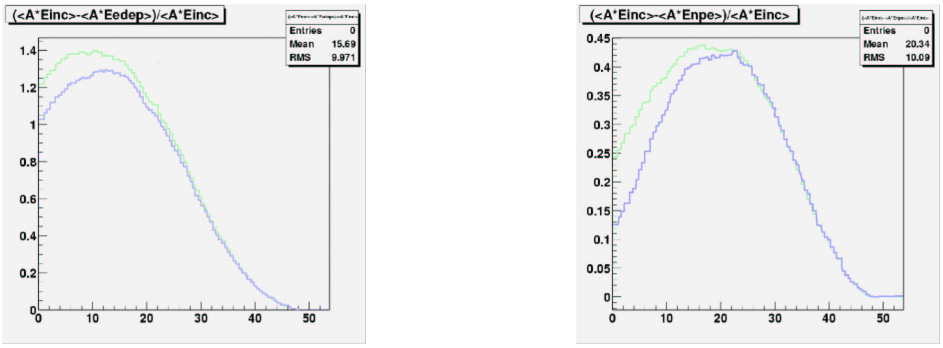

Figure 16: *$\delta A = (A_{Ei} - A_{Edet})/A_{Ei}$ versus detection threshold for a 1.2 GeV beam and green laser (Compton edge at 49 MeV). A_{Ei} is the mean analyzing power weighted by the incident photon energy and A_{Edet} is weighted by the energy deposited in the detector. Left: $PbWO_4$ crystal of 1 R_M, Right: 2 R_M. The blue curves include the statistical smearing of the light yield of the detector.*

2.3.4 Calorimeter Upgrade

Assuming the upgrade to a green laser we conclude the following about the photon detector for a 2% (or better) polarimetry:

- The semi-integrated method can be used at beam energies $\geq$ 2 GeV with the present setup. Increasing the transverse size of the active part of the detector from the central crystal to the 3×3 inner matrix would help. This requires either an accurate inter-calibration of the 9 crystals or a readout of the whole matrix by one bigger PMT.

- Below 2 GeV the use of the semi-integrated method requires the upgrade to a photon detector with a better resolution than $PbWO_4$ and a time response of few 100ns to reduce the pile up. The depth should be around 20 radiation lengths and the transverse size 2 R_M. We are investigating the possibility of using new materials like LSO or YAP which have very high light yield and short time response. Unfortunately the volume required for the calorimeter is large compared with the usual setups for lower energy gammas. At present, LSO crystals remain prohibitively expensive. Our preliminary design is based on a 9-cell YAP calorimeter with individual PMT's. Tentative cost estimate is \$k3.1 per channel. The new calorimeter will use the existing data acquisition electronics.

- The integrated and energy weighted method is the most promising (see next section). The requirements are met by standard inorganic scintillators like BGO. The integrating ADC should be based on the HAPPEx technology. Some electronic components need to be optimized to allow for lower frequency of the signal. This method could be implemented for all beam energies. Cost estimate for a new crystal and its readout is below \$k10.

2.4 Data Acquisition

The upgrade will use the existing data acquisition electronics and software to a large extent. Additional acquisition and analysis software are necessary for the integrating method at low energies. The control system for prototyping and bench tests will be LabView. The final setup in Hall A beamline will be controlled with EPICS. While much of the existing EPICS package will be reused, EPICS interface for the laser and cavity lock servo system need to be developed. In addition, a VME/Linux based test set up for detector tests and development of EPICS control software will be necessary.

3 Expected Performances

The expected performances at low energy of the two complementary polarimetry methods are discussed in this section.

3.1 Coincidence Analysis

The results achieved with the response function analysis at 4.5 GeV for the $N-\Delta$ and G_E^p experiments [1] are taken as a reference point to evolve the performances of the Compton polarimeter at different beam energy and laser wave length. The reference running conditions are: 40 minutes run duration, E=4.5 GeV, I=40 μA,

$P_e = 70\%$, $P_\gamma = 1500$ W and $\lambda = 1064$ nm.

The error budget of these measurements is summarized in Table 4. All errors are relative errors. The column labeled "Correl" refers to errors correlated from one run to another. They can be seen as normalization errors and don't depend on the run duration T. The "Uncorrel" column refers to errors non-correlated from one run to another. They behave like statistical errors and scale with $1/\sqrt{T}$. They are the only contribution to the total error when considering the *monitoring* of P_e, with no absolute reference. Figure 17 illustrates the expected error versus beam energy for the current setup, according the following procedure:

- The normalization error from laser polarization is constant over the whole energy range: $\delta A_{laser} = 0.45\%$.
- Beam current asymmetry can be kept negligible with respect to the Compton analyzing power.
- All other errors scale with the analyzing power for the same run duration and same beam current

$$\delta A \;=\; \delta A^{ref} \times \frac{AnaP^{ref}}{AnaP(E)} \;=\; \delta A^{ref} \times \frac{4.5}{E} \tag{14}$$

  This is justified by the following arguments for each error of table 4:

  - False asymmetries A_x from position and angles differences correlated with the helicity reversals only depend on beam properties. Then relative error scale with the analyzing power. The mean value of the distribution of A_x for all runs of $N-\Delta$ and G_E^p experiments is found to be compatible with zero. The width of this distribution is taken as the systematic error. It comes from the time limited accuracy of the BPMs measurements. Hence when averaging over a longer period of time this error will scale down as the statistical one. This convergence will be used at low energy to compensate the small analyzing power.
  - The total counting rate doesn't depend on the beam energy. Therefore dead time is expected to remain a the same level and the relative error to scale with the analyzing power.
  - The background level in the compton detectors is very sensitive to the beam tune. Signal over background ratio of 20 were already achieved in an energy range of 3.3 to 5.7 GeV. The need of a safety gap of $\simeq 4$ mm between the electron detector and the primary beam leads to a minimum operating energy of 2.5 GeV.

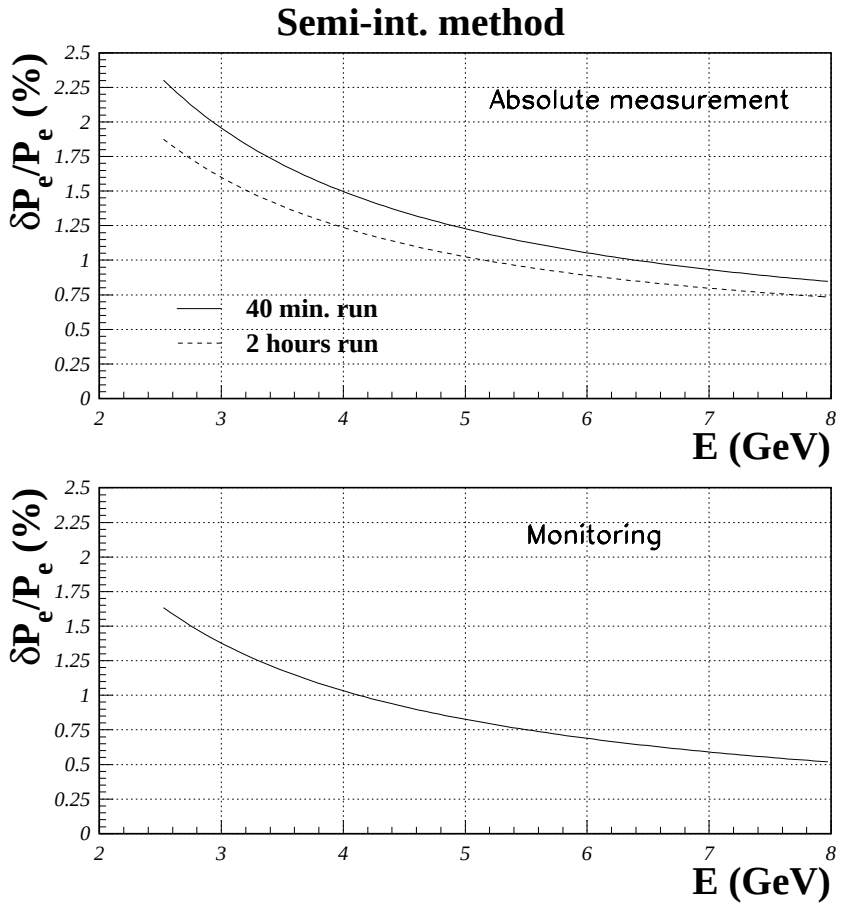

Figure 17: *Total relative error on the beam polarization for the semi-integrated method with the existing setup. The reference running conditions are taken from table 4 and evolution with beam energy follows the procedure described in the text. The monitoring error includes only the error not correlated from one run to another. The energy cut at 2.5 GeV is due to the limited operating range of the electron detector.*

– Evolving the error on the analyzing power versus beam energy is non trivial and requires a detailed simulation which is being developed. The relative errors coming from the parametrization and pile up might vary slower than linearly with the analyzing power. Therefore we believe that scaling with $1/E_{beam}$ as in eq.(14) is a safe estimate.

– The statistical error is proportional to the inverse square root of the running time. Because the integrated rate depends very little on the Compton kinematics (table 1), the relative error scales also with the analyzing power for a given run duration.

Table 4: Typical error budget of the "response function" analysis for a 40 minutes run with E=4.5 GeV, I=40 μA, P_γ = 1500 W and λ = 1064 nm. All errors are relative and $P_e \simeq 70\%$. The arrows indicate the expected error after the upgrade of the laser and the detectors with the same kinematics.

	Error source	Correl. (%)	Uncorrel. (%)
Laser	Polarization	0.45 → 0.30	
A_{exp}	Pos. and Angles		0.45 → 0.25
	Dead Time	0.10 → 0.10	
	Beam current asym.		0.05 → 0.05
	Background	0.05 → 0.05?	
Ana. Power	Calibration	0.60 → 0.30	
	Parameterization	0.45 → 0.45	
	Pile up	0.45 → 0.25	
Total Syst.		0.99 → 0.68	0.45 → 0.45
Stat.			0.80 → 0.40
Total		0.99 → 0.68	1.02 → 0.65

From figure 17 the HAPPEx2 requirement at 3 GeV (2% accuracy) is met. For accurate measurements at lower energy, we expect the following improvements based on the upgrades of the laser setup and detectors previously described:

- Laser polarization:
  In the present stage of the analysis, the observed variations in time of the laser polarization in the analyzing line are assumed to originate in the variations of the polarization at the CIP. In fact we know they could be due to a rotation of the polarization ellipse with no significant change of the degree of circular polarization. At the present stage of the analysis, the envelop of these variations is taken as a systematic error. A monitoring of the orien-

tation of the polarization ellipse would remove most of this uncertainty and bring the laser polarization error down to 0.3%.

- Dead time:
  The green laser setup is expected to double the light power accumulated inside the cavity so that for a two times smaller wave length the total counting rate stays the same. The dead time error is thus expected to remain small.

- Beam current asymmetry:
  The feedback developed for the parity experiments will keep the effect of the beam charge asymmetry negligible.

- Background:
  From our experience of data taking in 2000 and 2001, a signal to background ratio of 20 was routinely achieved over a beam energy range of 3.3 to 5.7 GeV. Data with the electron detector as close as 4.8 mm to the primary beam were taken with no evidence of beam halo. Although the high threshold ($\rho = 0.5$) of the semi-integrated method is an asset to reduce the background, at 850 MeV the electron detector must operate at 3.4 mm only from the primary beam. Data collected this year at this distance show the presence of a beam halo which could be due to an imperfect cut-off of the polarized source laser between two consecutive beam pulses. Assuming the beam halo can still be reduced smaller than the Compton rate at 3.4 mm from the beam centroid, then the ratio of the bremsstrahlung to Compton cross sections integrated from $\rho = 0.5$ to $\rho = 1$ doesn't depend on the beam energy to first order. We thus keep the error from the background constant and small (0.05%) with the caveat that beam halo properties must be demonstrated at low energy.

- Response function:
  The combined upgrades of the laser and electron detector should provide at least a factor 2 improvement in the calibration. Thus the relative error at 4.5 GeV becomes 0.30%.
  Because of the transition from pair creation to multiple Compton scattering in the photon detector, the error from the parametrization of the response function is difficult to scale to lower beam energy. A complete GEANT4 simulation, coupled to the ROOT based Compton analysis is being developed to address this issue. Meanwhile we keep a 0.45% relative error at 4.5 GeV despite the upgrade to a green laser.
  The pile up effect is presently estimated from simulation. It is not corrected and a 100% systematic error is assigned. More detailed simulation studies will reduce this error. The upgrade to a faster photon detector (few 100ns) will reduce the size of the effect itself. We quote a 0.25% relative error for

all energies since the total counting rate doesn't depend on the kinematics. To extrapolate at different beam energies we try two scenario which we believe define a reasonable envelop: the error on the analyzing power is either scaled with $1/E_{beam}$ (eq.14) or kept constant from the value at 4.5 GeV.

The final error budget of the semi-integrated method with the setup upgraded for the low energy measurements is show in table 4. The way the error evolves from the reference at 4.5 GeV to lower energy is shown on figure 18. The envelop defined by the two scenario of the error of the analyzing power becomes very large at low energy. At the present stage of this study, this uncertainty doesn't allow to conclude on the feasibility of an accurate measurement at 850 MeV using the semi-integrated method.

3.2 Integrated and energy weighted photon detection

In the previous sections we have shown that integrating the signal of the photon calorimeter between a low threshold and the Compton edge has numerous advantages for the reduction of the systematic errors. In the following we estimate the contribution of the different sources of error for a measurement at 850 MeV.

- We assume the same properties of the beam positions differences than for the measurement at 4.5 GeV (table4). The error is scaled with the ratio of the mean analyzing powers as taken in table 1

$$\delta A_X \;=\; 0.45\% \times \frac{\langle A \rangle_{4.5\,GeV,IR}}{\langle A_E \rangle_{0.85\,GeV,green}} \;=\; 0.45\% \times \frac{4.66}{1.47} \;=\; 1.40\% \qquad (15)$$

- The background from beam halo observed in the electron detector doesn't show up in the photon detector. This could be explained by the fact that in nominal running conditions a quadrupole upstream the Compton chicane focuses the beam in the horizontal direction. Indeed the limiting apertures for the Compton photons are narrow in the horizontal plane (± 5 mm) but quite large in the vertical plane ((± 25 mm)).
  Therefore we assume no major contribution from the beam halo in the photon detector and start with the signal over background ratio (S/B) measured at 4.5 GeV with a $\rho = 0.5$ threshold: $S/B \simeq 20$. Then the main contribution to the background is bremsstrahlung on the residual gas in the beam pipe which cross section can be written as

$$\frac{d\sigma}{dk} = \frac{A}{X_0 N_A} \frac{1}{k} \left(\frac{4}{3} - \frac{4}{3} \frac{k}{E_0} + \frac{k^2}{E_0^2} \right)$$

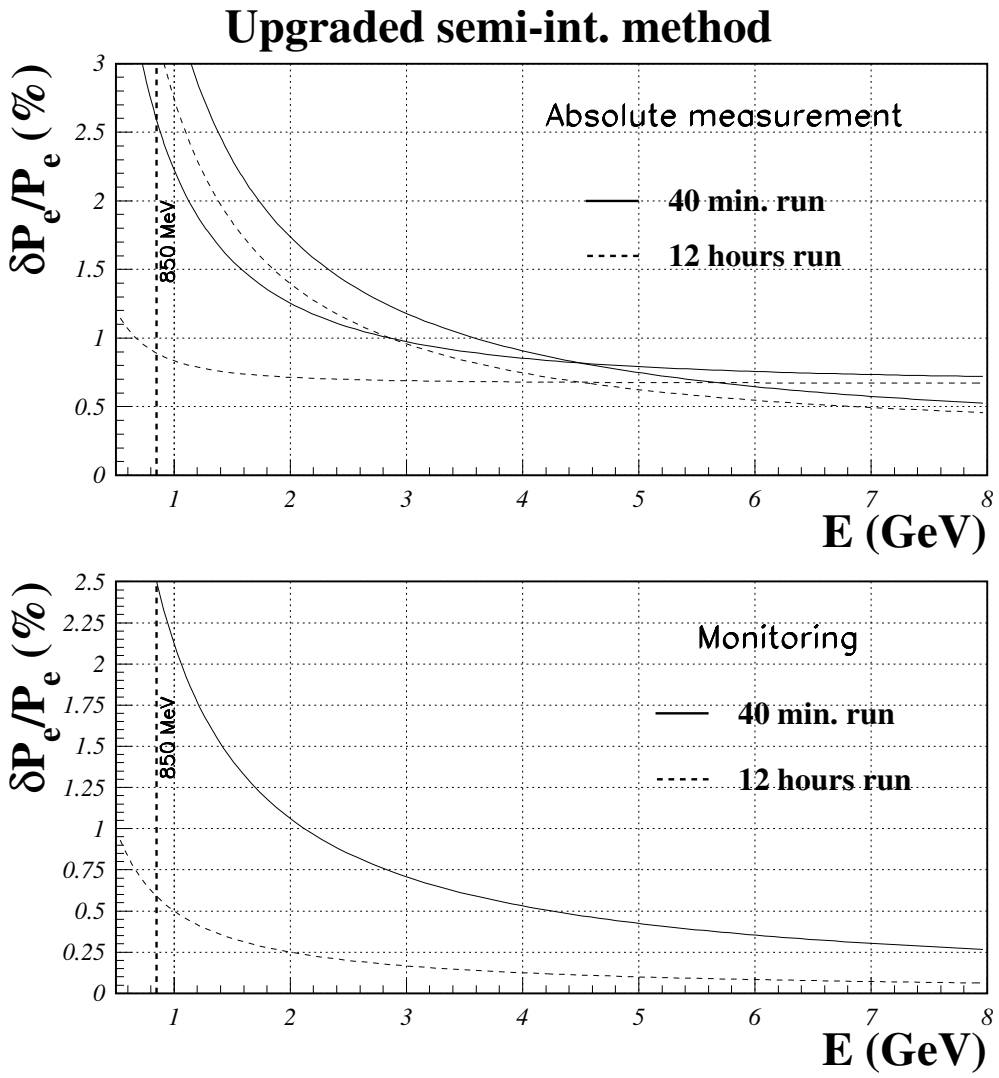

Figure 18: *Expected performances of the semi-integrated method with the upgraded polarimeter. Solid curves are for a 40 minutes run, dashed curves are for 1 day. The envelope defined by two curves of the same type comes from the two different ways of evolving the response function error versus beam energy (see text for details).*

where E_0 is the beam energy and k the energy of the radiated photon. Using this formula we can estimate S'/B' for the integrated and energy weighted method. The integration is performed from a null threshold up to E_0, the end of the bremsstrahlung spectrum

$$\frac{S'}{B'} = \frac{1}{2}\frac{E_{IR}}{E_{green}}\left(\frac{E}{E'}\right)^2 \frac{{k'_m}^2}{k'_e(k_m - k_t)} ln\frac{k_e}{k_t} \tag{16}$$

where the primed quantities refers to the $E' = 850$ MeV kinematics with green laser and the others to the reference conditions at E=4.5 GeV. k_m is the compton edge, $k_t \simeq k_m/2$ the threshold of the semi-integrated method and k_e the upper limit of the integration range. Using $k_e \simeq 2k_m$ and $k'_e \simeq E'$ one obtain

$$\frac{S'}{B'} \simeq \frac{S}{B} \times 0.042 \simeq 0.86$$

Hence we can't afford to integrate all the bremsstrahlung spectrum in our signal. One possibility would be to design a pre-amplifier to limit the pulse height send to the integrating ADC to an equivalent of let's say $k' = 2k'_m$ (50 MeV). The Compton events are not affected because this upper limit is far above the Compton edge. Moreover the rate of high energy bremsstrahlung events is low and pile up with a Compton event becomes very unlikely. Forcing the saturation at 50 MeV would bring the S'/B' ratio back to an acceptable value

$$\frac{S'}{B'} \simeq 15$$

The usual data taking procedure (2/3 cavity On, 1/3 cavity OFF) is still suitable for this level of background. We assume the relative error scales with S/B leading to $0.05\% \times 20/15 = 0.07\%$.

- From preliminary simulations, the response function of the detector never changes the mean analyzing power by more than 1%. Assuming a control of this effect at the 50% level we end up with 0.5%.

- The acquisition chain will have to be linear over an energy range of 0.25 to 25 MeV. Assuming a not corrected 3% non-linearity leads to a 0.30% error. Tagging the compton edge with the electron detector and using radioactive sources may be a way to check the linearity online.

- The main goal is to keep the detection threshold low enough so that we have a detection efficiency high and flat down to 1 MeV (fig.15). Then the threshold can be anywhere between 0 and 250 keV with no significant contribution to the error. We quote 0.25% which corresponds to the effect of a 1 MeV threshold.

Table 5: Typical error budget of a "integrated and energy weighed" measurement at 850 MeV with $P_\gamma = 3000$ W and $\lambda = 532$ nm. All other running conditions are identical to table 4.

	Error source	Correl. (%)	Uncorrel. (%)
Laser	Polarization	0.30	
A_{exp}	Pos. and Angles		0.33
	Background	0.07	
Ana. Power	Response func.	0.50	
	Linearity	0.30	
	Threshold	0.25	
Total Syst.		0.72	0.33
Stat.			0.82
Total		0.72	0.89

- The integrated method has no dead time. With a few 100 ns decay time of the detector the effect of pile up will be negligible.
- The control of the beam current asymmetry for the parity experiment is far beyond the Compton requirements.
- The statistical error scales with the inverse square root of the figure of merit. From table 1 we get $0.8\% \times \sqrt{13.2/0.69} = 3.5\%$.

The final error budget is show in table 5 were the uncorrelated errors has been calculated for a 12 hours run instead of 40 minutes. The correcting factor for these errors is thus $\sqrt{40}/\sqrt{12 \times 60} = 0.24$. Figure 19 shows that this method is promising for accurate measurements at low energy.

4 Cost and Schedule

We estimate the total equipment cost for the project to be 235 k$. An itemized cost list of components is shown in Table 6. For key items, we have consulted with appropriate vendors (as indicated in Table 6), who have provided us with actual quotations. The estimated cost does not include mechanical design work. Furthermore, there is no contingency built in to the cost estimate.

We estimate that the project can be completed in approximately two years provided adequate manpower is available from the Hall A Collaboration for the effort. The upgrade consists of five subsystems which can be pursued by separate groups: Fabry-Perot cavity, electron detector, photon calorimeter, DAQ, and

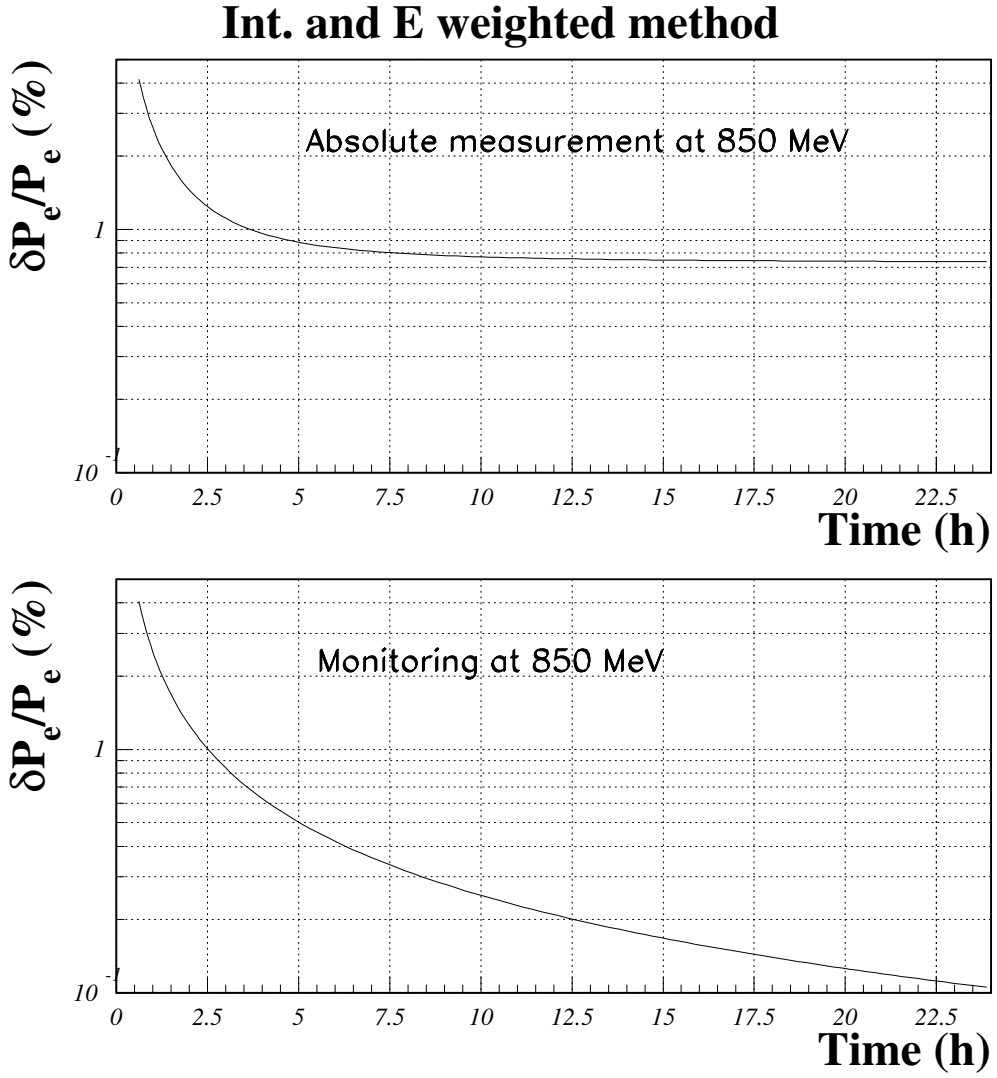

Figure 19: *Expected performances of the integrated and energy weighted method with the upgraded polarimeter. The beam energy is fixed at 850 MeV.*

Table 6: *Cost Estimate*

Item	Source	Model	Qty	Cost($)	Total
Laser					**54,200**
100 mW/532 nm Laser	Innolight	Prometheus	1	54,200	
Cavity					**30,790**
HR Mirrors	Research Electro-Optics	532 nm	12	6,900	
Lock-in Amplifier	Signal recovery	7280	1	8,000	
Modulator	Yokogawa	FG200	1	2,445	
Ramp Generator	HP	33120A	1	1,445	
Mechanical	Estimate			12,000	
Optics					**43,300**
Transport Mirrors	Newport		10	1,500	
Focusing lenses	Estimate		3	2,000	
polarizer plates	Estimate		4	2,800	
Beam Splitter	Estimate		3	2,500	
Photo Detectors	Estimate		4	2,800	
Faraday Isolator	LeySop	FOI 5/57	1	2,500	
Wollaston prism	LeySop	BSW-10	1	1,000	
Integrating spheres	Newport	819-IS-2	2	5,800	
Power Meter	Newport	2930-C	1	4,200	
Motorized mounts	PI	M-100	6	8,200	
Motion Controller	PI	C848	2	10,000	
Electron Detector					**30,000**
Mask	Canberra		1	10,000	
Microstrips	Canberra	250μ	4	10,000	
Motion control	Estimate			5,000	
Mechanical	Estimate			5,000	
Photon Detector					**40,000**
YAP Calorimeter	Estimate			30,000	
BGO Detector	Estimate			5,000	
Integrating Electronics	Estimate			5,000	
Control System					**11,300**
VME Crate				3,000	
IOC	Motorola	PPC2600	1	3,800	
Serial I/O Card	estimate			2,500	
Computer	estimate	Linux	1	2,000	
Test Setup					**25,800**
Oscilloscope	Tektronics	TDS3054B	1	10,600	
Optics Bench	Newport		1	4,400	
SHG startup kit	Alphalas		1	6,600	
Beam Profiler	Photon	21801	1	4,200	
Project Total					**235,390**

EPICS. We envision the cavity development to take place at Jefferson Lab while the two detectors could be pursued at other institutions.

4.0.1 Milestone Schedule

- Basic Laser lab setup May 2004
- Final design complete July 2004
- Green cavity prototype February 2005
- Calorimeter prototype May 2005
- Cavity installation in Hall A Summer 2005
- First measurements at >4 GeV Fall 2005
- Electron detector Installation Winter 2005
- Photon calorimeter Installation Winter 2005
- First measurement at <1 GeV Spring 2006

References

[1] S. Escoffier, *Mesure précise de la polarisation du faisceau d'électrons a TJNAF par polarimetrie Compton pour les expriences Gep et N-Delta*, PhD thesis, CEA-Saclay.

[2] G. Bardin *et al.*, Conceptual Design Report of a Compton Polarimeter for CEBAF Hall A, CEA-Saclay, 1996.

[3] H. Sakai *et al.*, Nucl. Inst. Meth.A445 (2000) 113.

[4] J. Urukawa *et al.*, Nucl. Inst. Meth.A 445, 113 (2000)

[5] M. Bregant *et al.*, arXIV:hep-ex/0202046 v1 28 Feb 2002.

[6] A. M. de Riva *et al.*Rev. Sci. Instrum. 67 (8), August 1996

[7] Optical Frequency Standard Development in Support of NASA's Gravity-Mapping Missions, W. M. Klipstein *et al.*http://esto.gsfc.nasa.gov/conferences/estc-2002/Papers/PS1P3(Klipstein).pdf

[8] G.C. Bjorklund *et al.*Appl. Phys. B 31, 145 (1983)

[9] D. Berns, Research Electro Optics, http://www.reoinc.com/

[10] I. Freitag, InnoLight GmbH, http://www.innolight.de/

[11] R. W. P. Drever *et al.*Appl. Phys. B 31, 145 (1983)